Acta Montanistica Slovaca
ISSN 1335-1788
actamont.tuke.sk

A dynamic model of a longwall shearer with a chain haulage system

*Łukasz BOŁOZ[1]**

Authors' affiliations and addresses:
[1]AGH University of Science and Technology, Department of Machinery Engineering and Transport, A. Mickiewicza Av. 30, 30-059 Krakow, Poland
e-mail: boloz@agh.edu.pl

***Correspondence:**
Łukasz Bołoz, AGH University of Science and Technology, Department of Machinery Engineering and Transport, A. Mickiewicza Av. 30, 30-059 Krakow, Poland
e-mail boloz@agh.edu.pl

How to cite this article:
Bołoz, L. (2022). Dynamic model of a longwall shearer with a chain haulage system. *Acta Montanistica Slovaca,* Volume 27 (3), 589-606.

DOI:
https://doi.org/10.46544/AMS.v27i3.03

Abstract
Despite the pro-ecological policy, hard coal still is and for a long time will remain a valuable major source of energy in the world. It is usually found in the form of seams in underground mines. For many years, thin coal seams have been exploited on an increasingly large scale; therefore, mines and machine manufacturers are looking for new, effective and safe methods of extraction. One such method is the use of a longwall system with a single-head shearer. This solution has been briefly described in the article, with special focus placed on the proprietary dynamic model of a longwall shearer with a chain haulage system**.** The model concerns a chain-hauled single-head shearer but can be used to simulate coal ploughs and scraper and belt conveyors to a certain extent. There are models in the literature in which the chain is replaced by point masses. In the discussed model, the chain segments have been described as a continuously distributed mass, the value of which changes as the shearer travels along the wall. The shearer has been modelled as a rigid body with six degrees of freedom, placed on elastic skids. The load from cutting, loading and movement resistance has been taken into account in the model. The mathematical model has been saved in the form of scripts in Matlab. The set of scripts allows obtaining information about the behaviour of the shearer and the load on important structural nodes such as skids, chain and loaders fasteners or the driving shaft of the cutting head. The results also enable determining the power demand of the motors as well as calculating the required initial tension of the chain. The fully parametric model makes it possible to analyse the influence of a change in the values of significant parameters of the longwall working, drive units and shearer. This information is crucial at the stage of design construction and verification, which allows for avoiding many errors in the prototype.

Keywords
machine dynamics, model tests, simulation tests, single-head shearer, chain haulage system, dynamic model, longwall shearer

Introduction

In recent years, coal mining in Europe has been treated as an energy source that should be quickly abandoned. However, in contrast to this approach, many countries around the world maintain hard coal mining at a high level (Saga, et al., 2020). The current energy crisis caused by the ongoing conflict and the sanctions imposed may change the policy of the European Union. In many countries, hard coal seams defined as medium and thick have been exhausted. Hard coal mines and manufacturers of mining machines are therefore becoming increasingly interested in the possibility of efficient exploitation of thin seams, i.e. ones with a thickness ranging from 1.0 m to 1.6 m. This situation results from a large amount of coal in such seams and the lack of appropriate machinery enabling their effective exploitation, especially under difficult mining and geological conditions. They are exploited, to a limited extent, by means of systems equipped with shearer or plough complexes.

In recent years, several machine solutions for thin seam exploitation have been developed based on longwall systems. In particular, the complex equipped with a single-cutting head shearer allows the disadvantages of the currently used ploughing and shearer systems to be largely eliminated (Bołoz, 2013). The solution of the system for exploiting thin seams is an example of innovation in the field of mining machines, which are important for industry development and competitiveness (Midor, 2017), (Zasadzień, 2015), (Bołoz and Biały, 2020). The implementation of this system provides an opportunity for Polish companies to create effective competition for longwall and plough systems.

Fig. 1 shows a longwall shearer complex consisting of a single-head shearer *1*, face conveyor *2*, power support *3*, and beam stage loader 4. At the ends of the face, the conveyor are located its drives *5*, and shearer drives *6* (Jakubowski, 2014).

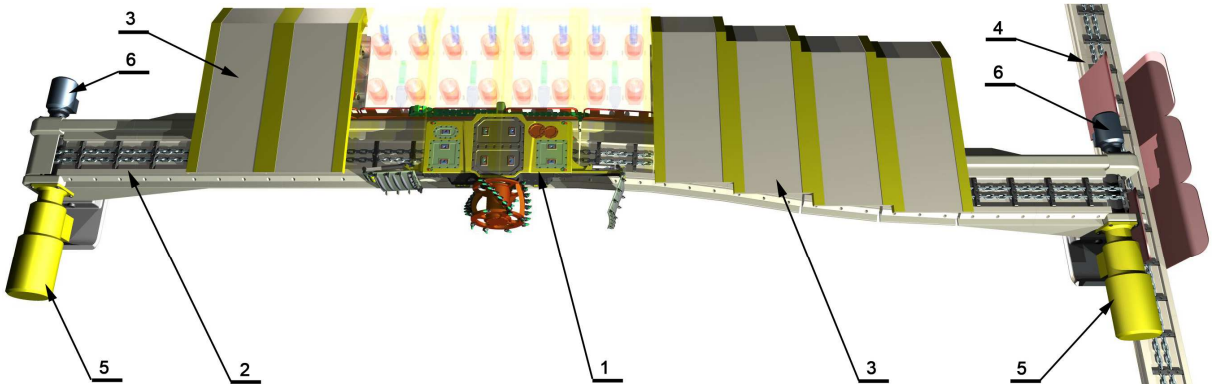

Fig. 1. Longwall system for the exploitation of thin seams

The shearer's body contains a head drive unit with a power of approx. 2x120 kW, which is equipped with appropriate planetary gear, protective devices, and a lubrication and cooling system (Saga, Blatnicky et al., 2020). The power was determined on the basis of reports concerning the consumption of power by the longwall shearer cutting head and the analysis of cutting resistance for the designed pick system (Litak, 2010), (Jonak et al., 2020). The load resulting from the cutting resistance can also be defined by determining the actual cutting resistance acting on the tool during empirical tests (Biały, 2014), (Biały, 2016). In addition to the drive unit, the body is equipped with a hydraulic system as well as automation, control and diagnostic systems. The necessary and required sprinkler system can be installed in the cutting head or, similarly to the plough technology, in longwall supports. An air-water system has been planned to reduce dustiness (Prostański, 2012, Abramov et al., 2015, Bozek et al., 2022).

Implementing the system prototype, which has no equivalent among the existing solutions, requires the development of a theoretical model and implementing model tests. Analytical and modelling testing is a highly developed field because, apart from the cognitive aspect, it allows for minimising potential errors in the prototype. Model tests provide important information that cannot be obtained in real object testing thanks to the possibility of testing many variants, including the ones with extreme and critical values of input parameters.

The issue of machine modelling is generally known in the literature (Karlinski et al., 2017), (Karlinski et al., 2020), (Derlukiewicz and Karlinski, 2012) (Kovanič et al., 2019), (Kovanič et al., 2020). Many dynamic models of various machines have been developed (Kovanič et al., 2021), including those with multiple degrees of freedom (Kouroussis et al., 2015), (Jedliński et al., 2022), (Bołoz, 2020). In numerous works, the object of the dynamic model was classic longwall shearers with two cutting heads and a chainless shearer haulage system (Saga et al., 2014). The aim of these studies was to analyse the possibilities of compensating for errors in the navigation system resulting from the work dynamics (Yang et al., 2016) or the influence of rock properties (Yang et al., 2021). In other articles, their authors modelled and studied the dynamics of the shearer's advance drive (Dolipski et al., 2012), (Zhang and Zhang, 2020), (Liu et al., 2015), (Kotwica et al., 2021).

In the subsequent article, the authors developed a dynamic model of a roadheader (Cheluszka et al., 2018). The influence of the regulated angular velocity of the cutting head was investigated. In another work, the same author studied the effect of the properties of the excavated rock while taking into account the automatic control of the process (Cheluszka, 2018).

Due to the nature of the work, the modelled systems are those used in processing machines. One example is the problem of vibrator synchronisation, where the behaviour of a dynamic model was simulated (Hou et al., 2016). In (Nikitin et al, 2020) (Peterka et al, 2020) logic-linguistic models were used for the diagnosis of electrical drives of machine tools.

Many publications present dynamic models of the scraper conveyor with a minimum of two drives and tension, where the chain is modelled as several point masses (Jiang et al., 2017). The authors study the dynamics of the conveyor or analyse the effect of unequal loading of the main and auxiliary drives (Dolipski et al., 2014). The scraper conveyor presented in other articles was modelled in a similar way, with the purpose of the simulation being the dynamics of toothed gears (Lohrengel et al., 2011).

Due to the way of moving, coal ploughs are similar to the discussed solution of the shearer. Coal ploughs with a chain haulage system are the subject of several studies, where they have been modelled as classic systems with a chain replaced by point masses (Li et al., 2010), (Kang and Li, 2010).

Also, belt conveyors are usually modelled as a series of point masses. In one of the papers, the authors investigated the transverse vibrations of the belt (Bortnowski et al., 2021, Sentyakov et al., 2020). In another one, the conveyor belt was modelled as a continuously distributed mass (Junxia and Xiaoxu, 2018). However, unlike the model described in this article, the belt in the above-mentioned paper was of constant length and weight. The authors studied the influence of various parameters on the dynamics of the conveyor's operation.

The works cited above present the model of a rigid body, a load from various processes, resistance to motion, as well as models of haulage system tension chains. However, in the solution presented in this article, several significant design differences prevent the use of existing models. The discussed longwall shearer cooperates with the face conveyor in the same way as the coal plough, but it is subject to completely different loads. The chain presented as a certain number of point masses limits the application of the model and does not allow simulating continuous motion for a specified period of time. In the considered case, the chain modelled as a continuously distributed mass with a variable value of individual segments allows simulating the start-up and advance of the shearer over the entire length of the longwall.

Single-cutting head shearer load

During operation, the shearer is subject to a number of loads. Fig. 2 shows a 3D model of the shearer together with a description of the key elements and the associated load, whereas Fig. 3 presents a diagram of its load with significant quantities. The *xyz* coordinate system is assumed to be at the shearer's centre of gravity. The forces, moments and torques acting in the direction and in relation to the *x, y, z* axes are marked in blue, red and green. The loads from the cutting process (P_{xo}, P_{yo}, P_{zo}, M_{xo}, M_{yo}, M_{zo}) and the loading process (P_{xl}, P_{yl}, P_{zl}, M_{xl}, M_{yl}, M_{zl}), which are active loads of the shearer, have been marked on the diagram. Additionally, the body, the cutting head and the loader are subject to gravity forces. Their components have been marked as G_x, G_y, G_z, G_{xo}, G_{yo}, G_{zo}, G_{xl1}, G_{yl1}, G_{zl1}, G_{xl2}, G_{yl2}, G_{zl2}, respectively. Force P_1 is a force in the active branch of the chain, whereas force P_2 – in the passive branch. The shearer moving along the guides generates pressure forces, lateral forces and the resulting frictional forces. The vertical reactions in the skids have been marked as N_1, N_2, N_3, N_4, respectively, and the lateral ones as B_1, B_2. In addition, these reactions induce frictional forces in the z-axis direction, which have been marked as T_1, T_2, T_3, T_4, accordingly, and frictional forces in the direction of the *y*-axis – marked as T_{b1}, T_{b2}, T_{b3}, T_{b4}. The diagram also shows significant linear dimensions and the angle of the loader position. Due to the expected low values, the load in the direction of the *y*-axis caused by the excavated material located between the sidewall and the shearer, as well as the force caused by the resistance to motion of the cable carrier, were neglected.

After making a number of assumptions, a physical model and, next, a complete mathematical model of the single-cutting head shearer with a chain haulage system were developed. Important symbols describing the shearer with drives are marked on the diagram of the physical model. Coordinates (x, y, z, φ), masses (m), mass moments of inertia (I), driving torques (M), resistance torques (M_o), elasticity coefficients (k), chain tension force (F) and chain resistance to motion (O) have been marked. The shearer has six degrees of freedom, while the sprockets only rotate.

Unlike classic longwall shearers, in this case, the cutting head does not carry out the loading process but only the cutting process. To calculate the resistance of the mining process with a single tool and to reduce the load on the entire head to the drive shaft, the author's model described in the literature was used (Bołoz and Castañeda, 2018).

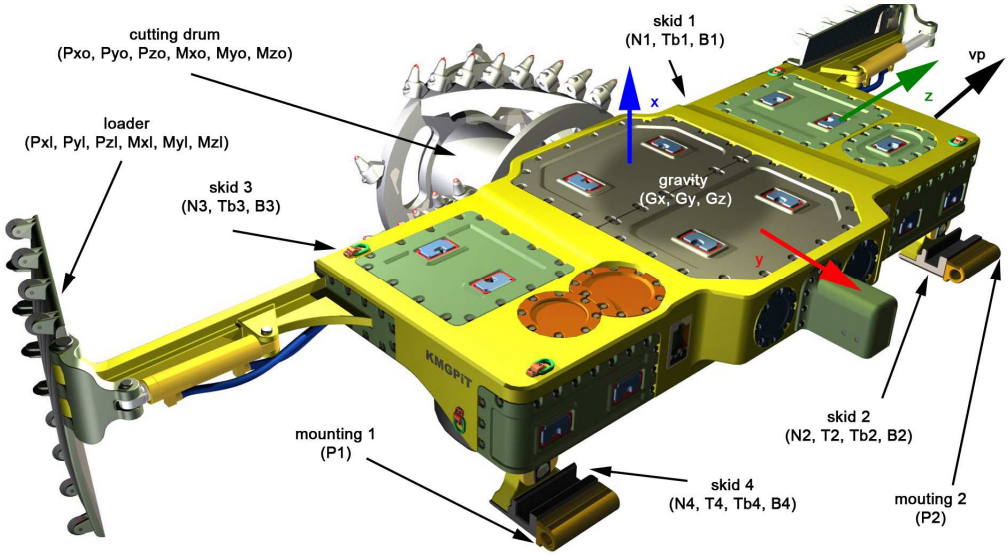

Fig. 2. Model of single-cutting head shearer

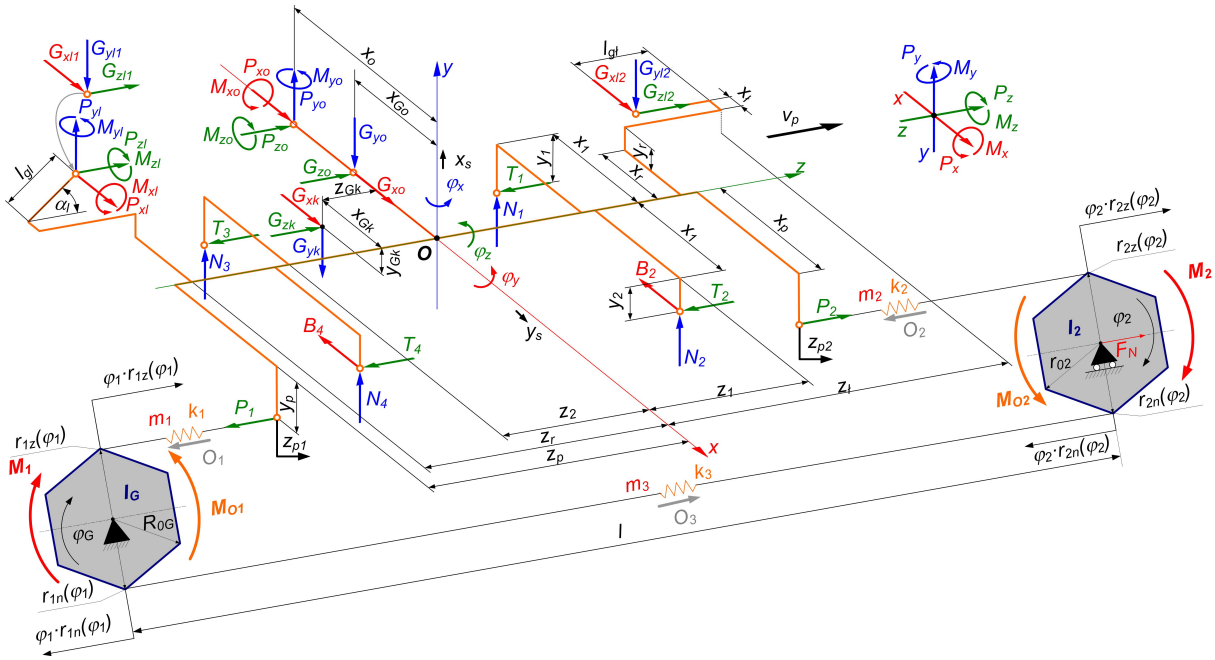

Fig. 3. Diagram of the single-cutting head shearer load (description of markings is given later in this article)

The process of loading with a cutting head involves winning, transporting the excavated material horizontally and vertically, as well as dumping it on the conveyor. In the discussed solution, the mined rock obtained in the cutting process is dumped on the conveyor by means of a loader (Fig. 4). The excavated material is left by the cutting head on the floor and, next, moved along the floor and along the loader surface towards the conveyor. During this movement, the mined rock generates resistance to motion against the floor, the sidewall and, if its amount is large, even against the roof. In addition, the internal friction resistance of the moving loose material and the friction against the loader surface, as well as the resistance resulting from the necessity to raise the spoil above the conveyor chute profile, should be taken into account.

This loading method is completely different from those currently used and until present has not been applied in longwall workings until the present. However, it is necessary to estimate the loading resistance of such a loader. Based on the physical dependences and the construction of the loader, the maximum mass of the spoil M_1 and the loading resistances were calculated:

$$P_{zl} = -2 \cdot \mu_{ws} \cdot M_l \cdot g \cdot \cos(\alpha_l) \tag{1}$$

$$P_{yl} = \mu_{wl} \cdot P_{zl} \cdot \sin(\alpha_l) \tag{2}$$

$$M_{yl} = 0.5 \cdot H \cdot P_{zl} \tag{3}$$

The presented data enable estimating the values of loading resistance, taking into account the most important parameters. It should be expected that the presented method of loading will be characterised by low dynamics, and the values of resistance that have been taken into consideration according to the adopted methodology are sufficient.

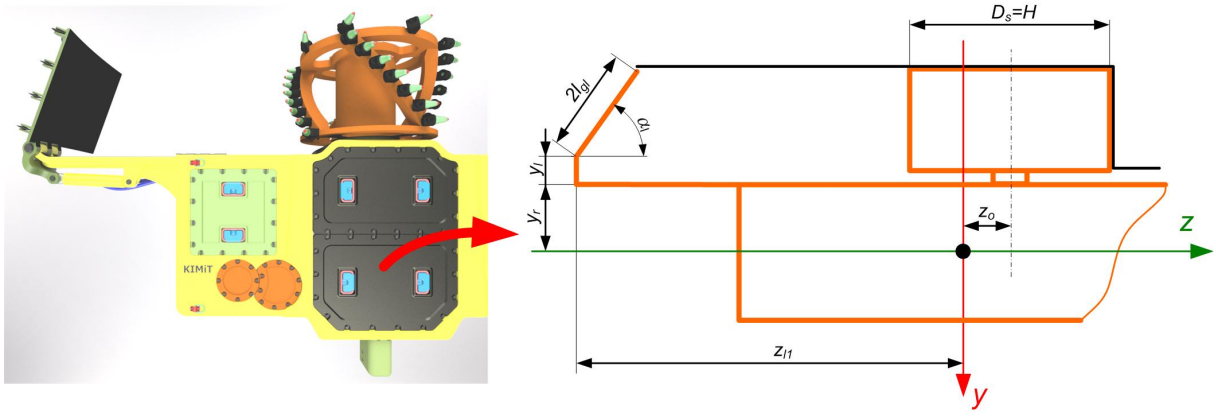

Fig. 4. Diagram for calculating the amount of loaded output

Load transferred via skids and drive

In addition to the load resulting from the process of cutting and loading, there are also frictional forces generated by the skids. The skid system is statically indeterminate. In this system, the shearer is supported on a plane at four points. Therefore, to solve this system, the values of skid stiffness k_x, k_y, k_z were introduced in three directions. Fig. 5 shows the adopted diagram of the skid's contact with the guide, assuming a specific stiffness and viscous damping c_x, c_y, c_z. The following dependencies for the frictional forces and the pressure force can be written:

$$N_1 = -k_x \cdot d_{x1} - c_x \cdot v_{x1} \quad \wedge \quad T_{b1} = k_y \cdot d_{y1} + c_y \cdot v_{y1} \quad \wedge \quad T_1 = k_z \cdot d_{z1} + c_z \cdot v_{z1} \tag{4}$$

Introducing the stiffness values in three directions for each skid allows the shearer to move freely. It has been assumed that the shearer's body, except the skids mentioned above, is a rigid body. The way the shearer is guided along the longwall by means of skids prevents the loss of stability; hence there is no need to analyse such a situation (Bołoz and Kozłowski, 2021).

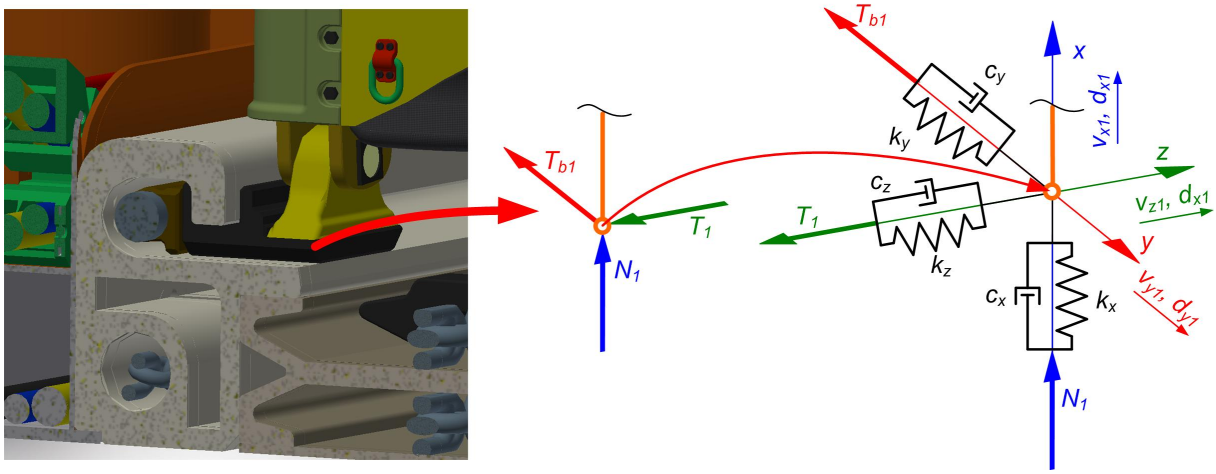

Fig. 5. Diagram of contact between the skid and the guides

Solids with six degrees of freedom can be analysed according to Euler's formula, using:

- three translational coordinates x_s, y_s, z_s of the centre of mass in the *xyz* fixed coordinate system,
- three angular coordinates φ, Ψ, Θ corresponding to Euler angles during rotation of the body around the mass centre. Taking into account a number of assumptions resulting from the construction of the shearer in question, we can write the equations of translational motion of its *mass* centre *and* Euler equations describing the rotary motion as:

$$m \cdot \ddot{x}_s = \sum P_{xi} \quad \wedge \quad m \cdot \ddot{y}_s = \sum P_{yi} \quad \wedge \quad m \cdot \ddot{z}_s = \sum P_{zi} \tag{5}$$

$$\begin{aligned} I_x \cdot \ddot{\varphi}_x - I_{xy} \cdot \ddot{\varphi}_y - I_{xz} \cdot \ddot{\varphi}_z &= \sum M_{xi} \\ I_y \cdot \ddot{\varphi}_y - I_{yx} \cdot \ddot{\varphi}_x - I_{yz} \cdot \ddot{\varphi}_z &= \sum M_{yi} \\ I_z \cdot \ddot{\varphi}_z - I_{zx} \cdot \ddot{\varphi}_x - I_{zy} \cdot \ddot{\varphi}_y &= \sum M_{zi} \end{aligned} \qquad (6)$$

where:

$I_{xy} = I_{yx}$, $I_{zx} = I_{xz}$, $I_{yz} = I_{zy}$ are the solid moments of deviation m in relation to the xyz axis of the system, calculated in the position of static equilibrium.

As a result, dynamic equations of the single-cutting head shearer motion can be derived, which can be expressed in the matrix form as:

$$\begin{bmatrix} m & 0 & 0 & 0 & 0 & 0 \\ 0 & m & 0 & 0 & 0 & 0 \\ 0 & 0 & m & 0 & 0 & 0 \\ 0 & 0 & 0 & I_x & 0 & 0 \\ 0 & 0 & 0 & 0 & I_y & 0 \\ 0 & 0 & 0 & 0 & 0 & I_z \end{bmatrix} \cdot \begin{bmatrix} \ddot{x}_s \\ \ddot{y}_s \\ \ddot{z}_s \\ \ddot{\varphi}_x \\ \ddot{\varphi}_y \\ \ddot{\varphi}_z \end{bmatrix} = \begin{bmatrix} P_x \\ P_y \\ P_x \\ M_x \\ M_y \\ M_z \end{bmatrix} \qquad (7)$$

The forces on the right side of the equation are the forces of external influences in the direction of the respective axes, while the moments are the moments of external influences in relation to respective axes. External loads are made up of reduced forces and moments resulting from cutting, loading and gravity, as well as skid friction forces, reactions in the skids and forces in the drive chain.

In order to determine the value of forces in the skids in accordance with the adopted formulas, it is necessary to determine the displacement of each skid. This displacement depends on the movement of the shearer's mass centre and its rotation. It is important that the shearer movement is understood as a free movement in space while taking into account the aforementioned six degrees of freedom.

The formula for displacement $\Delta r_{\varphi I}$ of any point as a result of the shearer's rotation by low values of angles $\Delta\varphi_x$, $\Delta\varphi_y$, $\Delta\varphi_z$ takes the following form:

$$\Delta\bar{r}_{\varphi i} = \hat{i}\left(\Delta\varphi_y z_i - \Delta\varphi_z y_i\right) + \hat{j}\left(\Delta\varphi_z x_i - \Delta\varphi_x z_i\right) + \hat{k}\left(\Delta\varphi_x y_i - \Delta\varphi_y x_i\right) \qquad (8)$$

By taking into account the movement of the shearer's mass centre and ignoring the Δ" sign (to facilitate the notation), we obtain dependences describing the displacement of any point of the shearer:

$$x_i = x_s + \varphi_y z_i - \varphi_z y_i \ \wedge\ y_i = y_s + \varphi_z x_i - \varphi_x z_i \ \wedge\ z_i = z_s + \varphi_x y_i - \varphi_y x_i \qquad (9)$$

The graphic interpretation of the formula has been given in Fig. 6 a. The presented formulas result from the addition of the vector of point P_i displacement and the vectors of mass centre displacement S.

Shearer's resistance to motion

Friction is an important physical phenomenon inherent in the operation of mechanical systems. Friction significantly affects durability, reliability and resistance to motion. In the present case, the friction model presented in the diagram in Fig. 6b has been used.

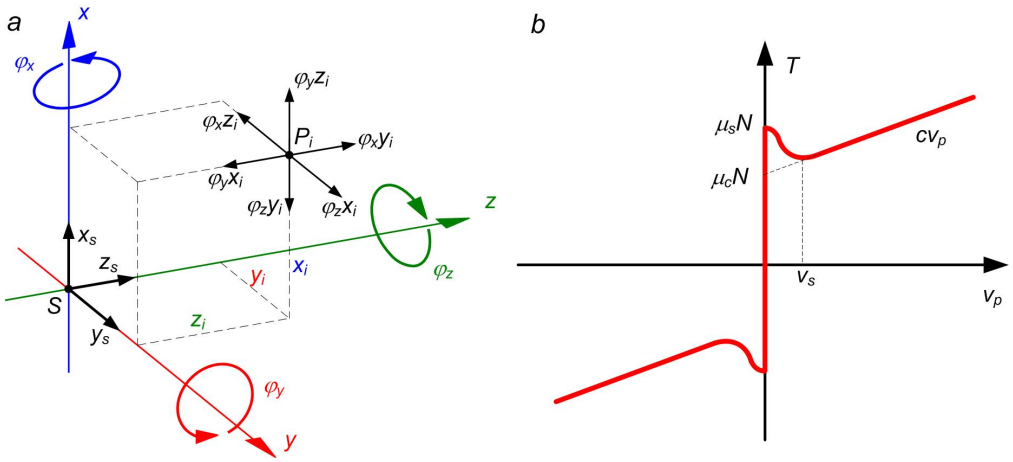

Fig. 6. Diagrams: a. displacement of any point of the solid in free motion, b. friction force according to selected models

In the initial phase, the friction force increases from zero to the value of maximum static friction. Then, the friction force decreases for Stribeck velocity v_s and, next, continues to increase linearly. The friction force curve, described by the characteristics shown in Fig. 6b, can be expressed using the following equation:

$$T(v)=\begin{cases}\pm T_s & : v=0\\ \left(T_c+(T_s-T_c)^{-\left(\frac{v}{v_s}\right)^2}+T_v|v|\right)sign(v) & : v\neq 0\end{cases} \quad [\mathrm{N}] \qquad (10)$$

where:

T_s – static friction force, N,
T_c – Coulomb friction force, N,
T_v – viscous friction force, N,
v_s – Stribeck velocity, m/s.

Physical model of the drive of a shearer with a chain haulage system

When creating a physical model of a shearer with two drives, the following assumptions were made:

- moments of inertia of rotating drive parts were reduced to the moments of inertia of the sprockets,
- individual segments of the chain were replaced by a spring of an appropriate length and modulus of elasticity; it has been taken into account that this spring can transfer only tensile loads,
- the replaced segments of the chain have a continuously and evenly distributed mass,
- due to the high ratio of mechanical transmissions, the flexibility of the clutches was neglected, leaving one degree of freedom of the drives.

The assumed physical model provided a basis for creating the mathematical model of a single-cutting head shearer with a chain haulage system. Important symbols describing the shearer with drives have been marked on the diagram of the physical model (Fig. 7).

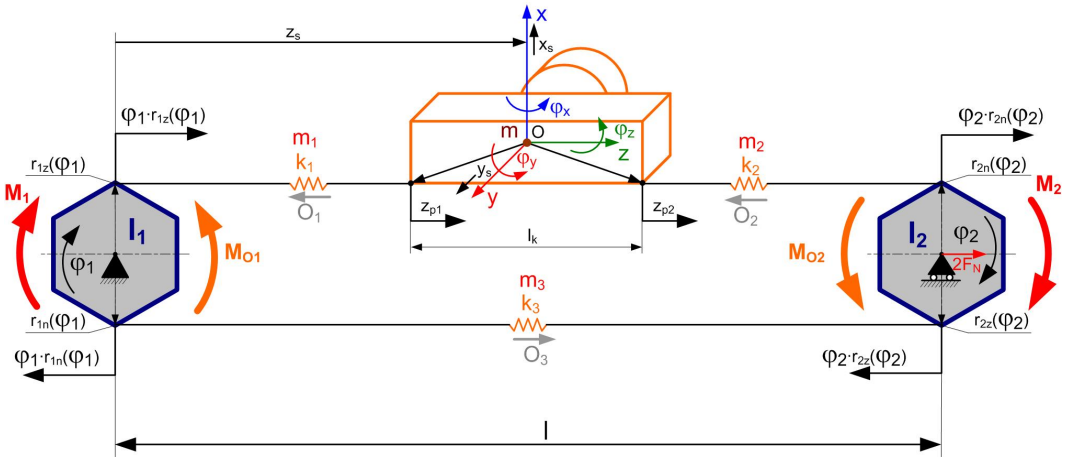

Fig. 7. Physical model of a single-cutting head shearer with a chain haulage system

Markings in Fig. 7:

x_s, y_s, z_s – displacement of shearer's mass centre towards the *x, y, z* axis,
φ_x, φ_y, φ_z – the angle of rotation of the shearer's body around the *x, y, z* axis,
z_{p1}, z_{p2} – displacement of the mounting points of the chain towards the axis *z* axis,
φ_1, φ_2 – rotation angle of the sprockets,
r_{1n}, r_{2n}, r_{1z}, r_{2z} – sprockets' input and output radiuses,
l – the distance between sprocket axes,
l_k – shearer length (distance between chain mounting points),
M_1, M_2 –drive torques reduced to the sprocket,
M_{O1}, M_{O2} – drive resistance to motion reduced to the sprocket,
$2F_N$ – initial tension of the chain,
$I_{1,2}$ – moments of inertia of the sprocket, motor rotor, reducer components and chain segment on the sprocket reduced to the output shaft described by φ_1, φ_2 coordinates,
m – shearer's mass,
m_1, m_2, m_3 – the mass of the chain segments l_1, l_2 (upper branch), l_3 (lower branch),

k_1, k_2, k_3 – equivalent coefficient of chain elasticity for chain segments l_1, l_2, l_3 ,
$O_{1,2,3}$ – resistance force generated by the chain m_1, m_2, m_3.

Dynamic equations of drive wheels motion

The sprocket mating with the drive chain has the shape of a polygon. Polygon modelling allows analysing the transverse movement of the chain and taking into account changes in the linear sprocket speed. Due to the purpose of the research and simplification of the model, the polygon has been replaced by a circle with an equivalent radius**:**

$$r_z = \frac{t \cdot z_k}{\pi} \ [m] \tag{11}$$

The dynamic equations of motion were determined on the basis of the physical model of the drive wheels presented in Fig. 8.

Equations of drive wheels motion resulted in the following:

$$\begin{aligned} I_1\dot{\omega}_1 &= M_1 + k_1\left(z_s + \varphi_x \cdot y_p + \varphi_y \cdot x_p - \varphi_1 \cdot r_1\right)r_1 + k_3\left(\varphi_2 \cdot r_2 - \varphi_1 \cdot r_1\right)r_1 \\ I_2\dot{\omega}_2 &= M_2 + k_2\left(z_s + \varphi_x \cdot y_p + \varphi_y \cdot x_p - \varphi_2 \cdot r_2\right)r_2 + k_3\left(\varphi_1 \cdot r_1 - \varphi_2 \cdot r_2\right)r_1 \end{aligned} \tag{12}$$

The mechanical characteristics of the asynchronous ring motor were expressed using the simplified Kloss formula. The elasticity coefficient of the chain appearing in the equations for a given variety and size depends on its length. Chain stiffness can be calculated from the following formula:

$$E_0 = \frac{F_{pl}}{\Delta l_l} \ [N] \tag{13}$$

where:

E_0 – chain stiffness, N,
F_{pl} – test load, N,
Δl_l – relative elongation under test load, m.

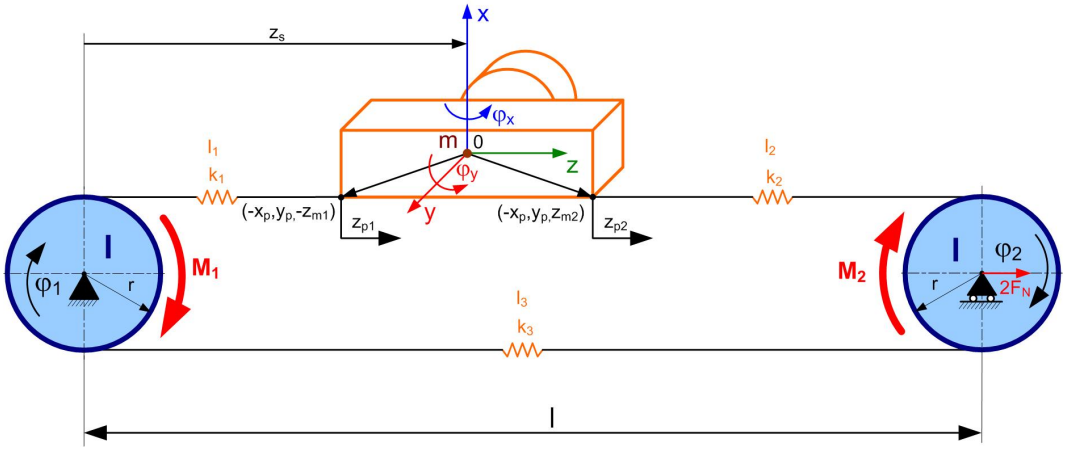

Fig. 8. Physical model for determining the dynamic equations of drive wheels motion

The elasticity coefficient of the chain k_1, which is required for calculations for its specific length l_1 can be calculated as the quotient of the stiffness to its length:

$$k_l = \frac{E_0}{l_l} \ \left[\frac{N}{m}\right] \tag{14}$$

where:

k_l – elasticity coefficient for a chain segment having length l_l, *N/m*,
l_l – chain length, *m*,

The lengths of individual segments of the chain can be determined by taking into account the following assumptions, which result from the nature of the machine operation (Fig. 8):

- the initial position of the shearer over the longwall length corresponds to an adequate rotation of the drive wheels,
- segment length l_1 results from the angle of rotation of the first drive wheel and is:

$$l_1 = \varphi_1 \cdot r \quad [m] \tag{15}$$

- segment length l_2 results from the angle of rotation of the second drive wheel and is:

$$l_2 = l - l_k - \varphi_2 \cdot r \quad [m] \tag{16}$$

- segment length l_3 results from the angle of rotation of the first and second drive wheels and longwall length. It equals:

$$l_3 = l + \varphi_2 \cdot r - \varphi_1 \cdot r \quad [m] \tag{17}$$

For the adopted assumptions, the coefficients of elasticity of individual chain segments are as follows:

$$k_1 = \frac{E_0}{\varphi_1 \cdot r} \left[\frac{N}{m}\right]$$

$$k_2 = \frac{E_0}{l - l_k - \varphi_2 \cdot r} \left[\frac{N}{m}\right] \tag{18}$$

$$k_3 = \frac{E_0}{l + \varphi_2 \cdot r - \varphi_1 \cdot r} \left[\frac{N}{m}\right]$$

The initial tension of the chain $2F_N$ is a static load designed to compensate for elastic elongations appearing during its operation (Tlach et al., 2019). The initial tension value should prevent the chain from slackening during the machine's operation.

It is assumed that the distance between the axes of the sprockets adopted for simulation takes into account the chain's elongation caused by the initial tension (Segota et al., 2020). To check whether the chain is not slack, an appropriate condition should be specified. The state of the chain should be checked for each of its segments. This condition takes the form of the following inequalities**:**

$$z_s + \varphi_x \cdot y_p + \varphi_y \cdot x_p - \varphi_1 \cdot r > -\frac{F_N}{k_1}$$

$$\varphi_2 \cdot r_2 - \left(z_s + \varphi_x \cdot y_p + \varphi_y \cdot x_p\right) > -\frac{F_N}{k_2} \tag{19}$$

$$\varphi_1 \cdot r_1 - \varphi_2 \cdot r_2 > -\frac{F_N}{k_3}$$

Model of a chain with a continuously distributed mass

The next stage of work was to take into account the kinetic energy of the chain, assuming that its individual segments had variable masses (Kuric et al., 2021). The variable mass results from the shearer's position, which changes during the cutting process, and from the angular displacement of sprockets.

The problem of describing variable mass systems by means of Lagrange's equations of the second kind has been discussed in the literature relatively recently (Saga et al., 2014). The authors (Pesce et al., 2006), (Pesce, 2011), (Bedoustani et al., 2011), among others, described systems with a variable mass resulting from the unwinding of the cable. These publications have demonstrated that commonly used Lagrange equations of the second kind require taking into account appropriate corrective components that enable a correct description of systems with variable masses.

In the case under consideration, the chain segments change their mass, but the mass of the entire system remains constant (Sapietova et al., 2011). Therefore, Lagrange equations of the second kind can be used to analyse the entire system without corrective components. In the discussed case, the Lagrange equation of the second kind takes the following form:

$$\frac{d}{dt}\frac{\partial E_k}{\partial \dot{q}_i} - \frac{\partial E_k}{\partial q_i} = Q_i \tag{20}$$

where:

E_k – kinetic energy,
Q_i – i-th generalised force,
q_i – i-th generalised coordinate.

The generalised coordinates are: displacement in the cutting direction z_s, rotations φ_x and φ_y of the shearer in relation to its mass centre, as well as rotations φ_1 and φ_2 of the sprockets.

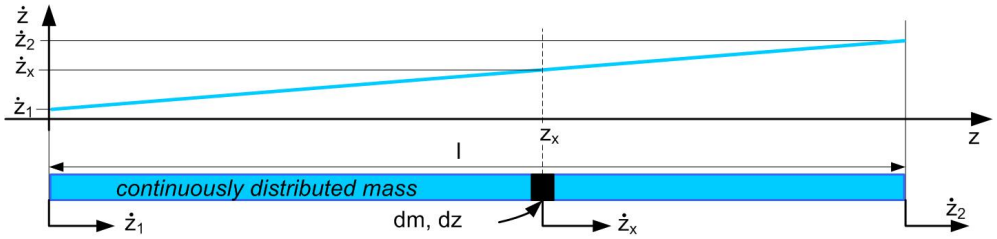

Fig. 9. Auxiliary diagram for deriving the kinetic energy of a body with a continuously distributed mass

Considering individual segments of a chain with a continuously distributed mass requires deriving the formula for the kinetic energy of such an element (Handrik et al., 2017). Fig. 9 shows a body with a continuously distributed mass m, linear density ρ and length l. Its beginning moves at speed $\dot{z}_1$ and the end at speed $\dot{z}_2$. In the state of static equilibrium, the linear density of the body is constant along its entire length. Speed over length l varies linearly (Kuric et al., 2022).

The analysis of the speed of any chain segment having length dz and mass dm resulted in the following relationship:

$$\dot{z}_x = \dot{z}_1 + \frac{\dot{z}_2 - \dot{z}_1}{l} \tag{21}$$

Knowing the speed and mass of the analysed segment, we can express its kinetic energy as follows:

$$dE_k = \frac{1}{2} dm \cdot \dot{z}_1^2 \;\Rightarrow\; dE_k = \frac{1}{2} dz \cdot \rho \cdot \dot{z}_1^2 \tag{22}$$

Hence, the kinetic energy can be expressed as:

$$E_k = \frac{1}{2}\rho \cdot \int_0^l \dot{z}_x^2 dz \Rightarrow E_k = \frac{1}{2}\rho \cdot \int_0^l \left(\dot{z}_1 + \frac{\dot{z}_2 - \dot{z}_1}{l} \right)^2 dz \tag{23}$$

After integration, the following is obtained:

$$E_k = \frac{1}{6} m \left(\dot{z}_1^2 + \dot{z}_1 \cdot \dot{z}_2 + \dot{z}_2^2 \right) \tag{24}$$

Fig. 10 shows the model of a shearer with a chain haulage system with distinguished individual chain segments having a continuously and evenly distributed mass (Kuric et al., 2020).

The segment having mass m_1 stretches from the sprocket to the hitch on the shearer's body; so does the segment having mass m_2. The lower branch of the chain having mass m_3 is located between the sprockets.

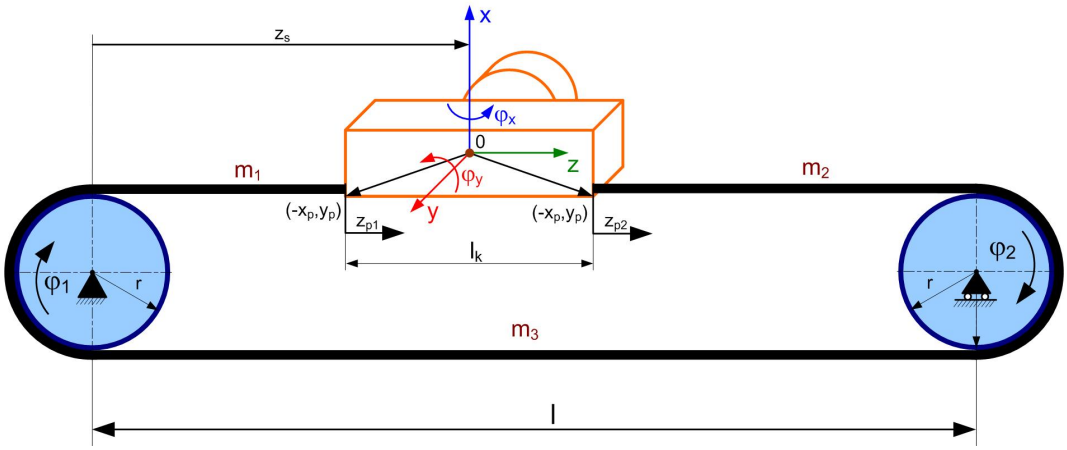

Fig. 10. Physical model taking into account the mass of the chain

The kinetic energy of the so-adopted system is:

$$E_k = \frac{1}{6} m_1 \left(\dot{z}_{p1}^2 + \dot{\varphi}_1^2 r^2 + \dot{\varphi}_1 \dot{z}_{p1} r \right) + \frac{1}{6} m_2 \left(\dot{z}_{p2}^2 + \dot{\varphi}_2^2 r^2 + \dot{\varphi}_2 \dot{z}_{p2} r \right) \ldots$$
$$+ \frac{1}{6} m_3 \left(\dot{\varphi}_1^2 r^2 + \dot{\varphi}_2^2 r^2 + \dot{\varphi}_1 \dot{\varphi}_2 r^2 \right) \tag{25}$$

The change in the weight of individual segments results from the chain rolling over the sprocket. When the sprocket rotates by value $\Delta\varphi_1$, mass m_1 increases by $r\rho\Delta\varphi_1$, whereas mass m_3 is decreased by the same value. It should be noted that the shearer's vibrations in direction z change the length of the chain in front of and behind the shearer but do not affect its weight (Abd Ali et al., 2021), merely causing its smaller or greater elongation (Muravev et al., 2019). In accordance with the markings given in Fig. 10, the dependences for m_1, m_2 and m_3 can be expressed as follows:

$$m_1 = \rho r\varphi_1 \ \wedge\ m_2 = \rho\left(l - l_k - \varphi_2 r\right) \ \wedge\ m_3 = \rho\left(l + \varphi_2 r - \varphi_1 r\right) \tag{26}$$

The speed $\dot{z}_{p1}$, $\dot{z}_{p2}$ of the chain hitches on the body can be expressed on the basis of the dependences given above and markings in Fig. 10:

$$\dot{z}_{p1} = \dot{z}_{p2} = \dot{z}_s + \dot{\varphi}_x \cdot y_p + \dot{\varphi}_y \cdot x_p \tag{27}$$

Therefore, the formula for kinetic energy has been expressed as:

$$\begin{aligned} E_k = {} & \frac{1}{6}\rho\varphi_1 r\begin{bmatrix}\left(\dot{z}_s + \dot{\varphi}_x \cdot y_p + \dot{\varphi}_y \cdot x_p\right)^2 + \dot{\varphi}_1^2 r^2 \ldots \\ +\dot{\varphi}_1 r\left(\dot{z}_s + \dot{\varphi}_x \cdot y_p + \dot{\varphi}_y \cdot x_p\right)\end{bmatrix}\ldots \\ & + \frac{1}{6}\rho\left(l - l_k - \varphi_2 r\right)\begin{bmatrix}\left(\dot{z}_s + \dot{\varphi}_x \cdot y_p + \dot{\varphi}_y \cdot x_p\right)^2 \ldots \\ +\dot{\varphi}_2^2 r^2 + \dot{\varphi}_2 r\left(\dot{z}_s + \dot{\varphi}_x \cdot y_p + \dot{\varphi}_y \cdot x_p\right)\end{bmatrix}\ldots \\ & + \frac{1}{6}\rho\left(l + \varphi_2 r - \varphi_1 r\right)\left(\dot{\varphi}_1^2 r^2 + \dot{\varphi}_2^2 r^2 + \dot{\varphi}_1\dot{\varphi}_2 r^2\right) \end{aligned} \tag{28}$$

After necessary calculations and transformations were performed, five dynamics equations were obtained, which can be expressed in a matrix form.

$$M \cdot \ddot{q} = Q \tag{29}$$

where:

M – mass matrix,

$\ddot{q}$ – vector of linear and angular accelerations,

Q – vector of loads.

Chain and drive resistance to motion

The above presented model of friction was also used to describe the resistances generated by individual chain branches. Fig. 11 shows a diagram of the resistance to the motion adopted for the analysis.

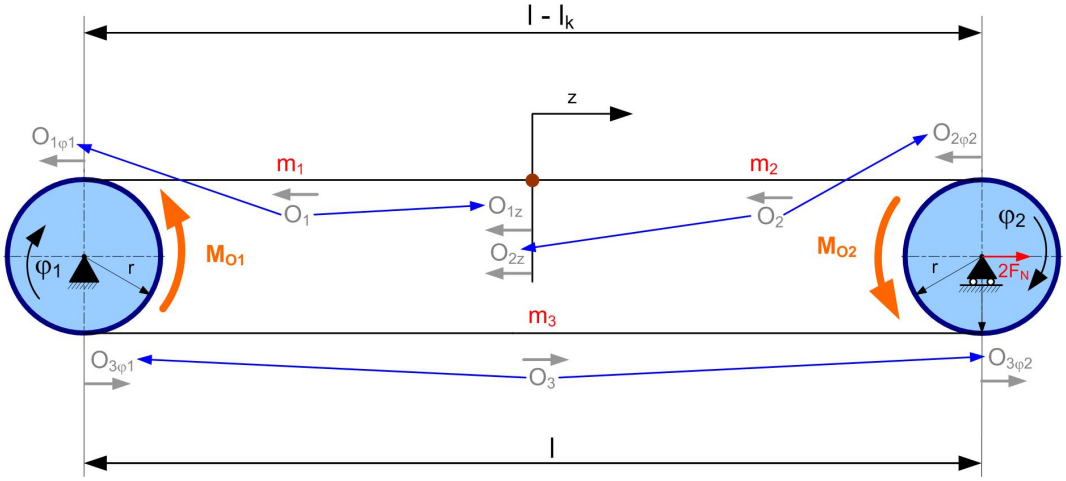

Fig. 11. Diagram for determining the chain and drives' resistance to motion

The resistances M_{O1} and M_{O2} were assumed as constant values, resulting from the efficiency of the drives. Determining the values of chain resistance to motion O_1, O_2, O_3 is a more complex problem. If the speed of the start of the chain is opposite to that of its end, then a part of the chain generates a frictional force opposite to that of the remaining chain (Klarák et al., 2022). In the analysed case, the speeds of the generalised variables are

positive. However, according to the definition of generalised force, the influence of the frictional resistance of individual chain branches on appropriate coordinates $O_{1\varphi 1}$, $O_{3\varphi 1}$, $O_{2\varphi 2}$, $O_{3\varphi 2}$, O_{1z}, O_{2z} should be determined. The generalised force formula is as follows:

$$O_{nj} = \sum_{i=1}^{m} T_{ni} \cdot \frac{\partial \overline{r}_{ni}}{\partial q_{nj}} \tag{30}$$

where:

O_{nj} –generalised force related to j-th coordinate acting on n-th segment,
m – number of forces acting on the system,
T_{ni} – friction force applied at point r_{nj},
j – number of generalised coordinates for n-th segment,
n –analysed segment of the chain.

The values of generalised forces acting on individual generalised coordinates should be determined for each of the three segments of the chain. Fig. 12 shows a diagram for determining generalised forces values. The length of the segment with point mass dm_{1i} is described by coordinates φ_1 and z. The length of the segment having point mass dm_{2i} is described by coordinates z and φ_1. The length of the segment having point mass dm_{3i} is described by coordinates φ_1 and φ_2. In the position determined by coordinate r_{ni}, the chain segment having a given mass dm_{ni} and length $d\xi_n$ is considered. The dm_{ni} segment generates friction force dT_{ni} and may be displaced by the dr_{ni} value. For each of the segments, the formula for r_{ni} has been determined:

$$r_{1i} = \varphi_1 r + \frac{z - \varphi_1 r}{z}\xi \;\wedge\; r_{2i} = z + (\varphi_2 r - z)\frac{\xi - z}{l - l_k - z} \;\wedge\; r_{3i} = \varphi_2 r + \frac{\varphi_1 r - \varphi_2 r}{l}\xi \tag{31}$$

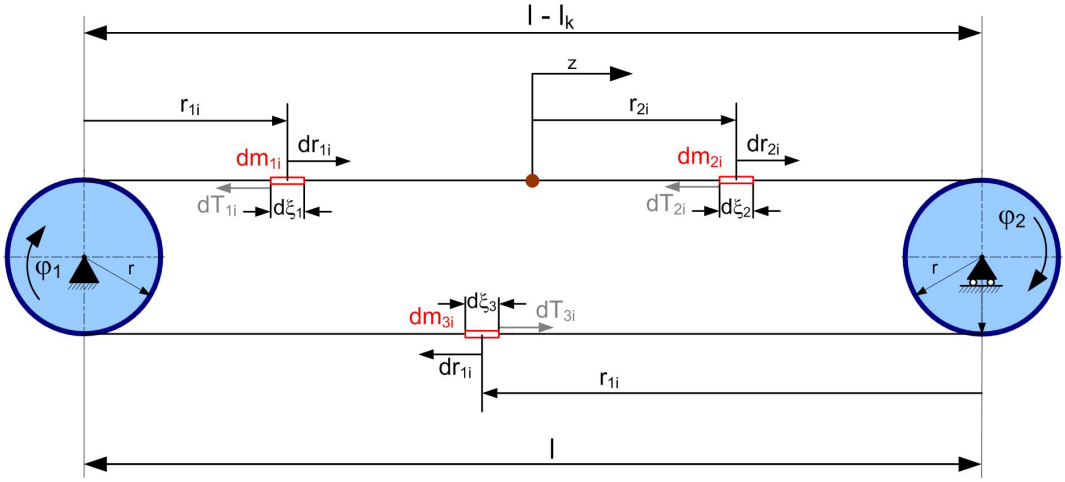

Fig. 12. Auxiliary drawing for determining the values of generalised forces

Changing their values, generalised coordinates influence the chain density:

$$\rho_1 = \frac{\varphi_1 r}{z}\rho \;\wedge\; \rho_2 = \frac{l - l_k - \varphi_2 r}{l - l_k - z}\rho \;\wedge\; \rho_3 = \frac{\varphi_2 r - \varphi_1 r + l}{l}\rho \tag{32}$$

Therefore, the values of frictional forces generated by the point masses of the chain can be expressed as:

$$dT_{ni} = g\mu\rho_n d\xi \tag{33}$$

For each segment of the chain, derivatives r_i were calculated with respect to the coordinates describing it. Next, the values of generalised forces applied to these coordinates were calculated. Calculations of derivatives and integrals were performed in the MathCad program (Kopas et al., 2017). The values of the forces, in accordance with the designations adopted in Fig. 11, are as follows:

$$O_{1\varphi 1} = g\rho_1\mu r\frac{z}{2}, \qquad O_{1z} = g\rho_1\mu\frac{\varphi_1 r}{2}$$
$$O_{2z} = g\rho_2\mu\frac{l - l_k - \varphi_2 r}{2}, \quad O_{2\varphi 2} = g\rho_2\mu r\frac{l - l_k - z}{2} \tag{34}$$
$$O_{3\varphi 2} = g\rho_3\mu r\frac{l}{2}, \qquad O_{3\varphi 1} = g\rho_3\mu r\frac{l}{2}$$

The obtained force values are close to half of the friction force value determined for the entire length of a given branch. Depending on the model used, the friction coefficient μ should be replaced by appropriate dependencies.

The presented considerations enabled constructing a complete dynamic model of the physical and mathematical load of a single-cutting head shearer, taking into account the chain haulage system. Taking into consideration the chain resistance to motion acting on the sprockets, the dynamic equations of the drive wheels can be expressed as follows:

$$\begin{aligned} I_1\dot{\omega}_1 &= M_1 + k_1\left(z_s + \varphi_x \cdot y_p + \varphi_y \cdot x_p - \varphi_1 \cdot r_1\right)r_1 \ldots \\ &\quad + k_3\left(\varphi_2 \cdot r_2 - \varphi_1 \cdot r_1\right)r_1 - O_{1\varphi 1} - O_{3\varphi 1} \\ I_2\dot{\omega}_2 &= M_2 + k_2\left(z_s + \varphi_x \cdot y_p + \varphi_y \cdot x_p - \varphi_2 \cdot r_2\right)r_2 \ldots \\ &\quad + k_3\left(\varphi_1 \cdot r_1 - \varphi_2 \cdot r_2\right)r_1 - O_{2\varphi 2} - O_{3\varphi 2} \end{aligned} \tag{35}$$

whereas the matrix equation of motion takes the form 36. The Q vector appearing in the above equation can be expressed as formula 37. The P_x, P_y, P_z, M_x, M_y, M_z loads in the Q vector take into account the cutting, loading and gravity resistance as well as loads resulting from the pressure of the skids and resistance to motion.

$$\begin{bmatrix} m & 0 & 0 & 0 & 0 \\ 0 & m & 0 & 0 & 0 \\ 0 & 0 & m+\frac{1}{3}\rho\varphi_1 r+\frac{1}{3}\rho\left(l-l_k-\varphi_2 r\right) & \frac{1}{3}\rho\varphi_1 y_p r+\frac{1}{3}\rho\left(l-l_k-\varphi_2 r\right)y_p & \frac{1}{3}\rho\varphi_1 x_p r+\frac{1}{3}\rho\left(l-l_k-\varphi_2 r\right)x_p \\ 0 & 0 & \frac{1}{3}\rho\varphi_1 y_p r+\frac{1}{3}\rho\left(l-l_k-\varphi_2 r\right)y_p & I_x+\frac{1}{3}\rho\varphi_1 y_p^2 r+\frac{1}{3}\rho\left(l-l_k-\varphi_2 r\right)y_p^2 & \frac{1}{3}\rho\varphi_1 x_p y_p r+\frac{1}{3}\rho\left(l-l_k-\varphi_2 r\right)x_p y_p \\ 0 & 0 & \frac{1}{3}\rho\varphi_1 x_p r+\frac{1}{3}\rho\left(l-l_k-\varphi_2 r\right)x_p & \frac{1}{3}\rho\varphi_1 y_p x_p r+\frac{1}{3}\rho\left(l-l_k-\varphi_2 r\right)y_p x_p & I_y+\frac{1}{3}\rho\varphi_1 x_p^2 r+\frac{1}{3}\rho\left(l-l_k-\varphi_2 r\right)x_p^2 \cdots \\ 0 & 0 & 0 & 0 & 0 \\ 0 & 0 & \frac{1}{6}\rho\varphi_1 r^2 & \frac{1}{6}\rho\varphi_1 y_p r^2 & \frac{1}{6}\rho\varphi_1 x_p r^2 \\ 0 & 0 & \frac{1}{6}\rho\left(l-l_k-\varphi_2 r\right)r & \frac{1}{6}\rho\left(l-l_k-\varphi_2 r\right)y_p r & \frac{1}{6}\rho\left(l-l_k-\varphi_2 r\right)x_p r \end{bmatrix}$$

$$\begin{bmatrix} 0 & 0 & 0 \\ 0 & 0 & 0 \\ 0 & \frac{1}{6}\rho\varphi_1 r^2 & \frac{1}{6}\rho\left(l-l_k-\varphi_2 r\right)r \\ 0 & \frac{1}{6}\rho\varphi_1 y_p r^2 & \frac{1}{6}\rho\left(l-l_k-\varphi_2 r\right)y_p r \\ 0 & \frac{1}{6}\rho\varphi_1 x_p r^2 & \frac{1}{6}\rho\left(l-l_k-\varphi_2 r\right)x_p r \\ I_z & 0 & 0 \\ 0 & I_1+\frac{1}{3}\rho\left(l+\varphi_2 r\right)r^2 & \frac{1}{6}\rho\left(l+\varphi_2 r-\varphi_1 r\right)r^2 \\ 0 & \frac{1}{6}\rho\left(l+\varphi_2 r-\varphi_1 r\right)r^2 & I_2+\frac{1}{3}\rho\left(2l-l_k-\varphi_1 r\right)r^2 \end{bmatrix} \cdot \begin{bmatrix} \ddot{x}_s \\ \ddot{y}_s \\ \ddot{z}_s \\ \ddot{\varphi}_x \\ \ddot{\varphi}_y \\ \ddot{\varphi}_z \\ \ddot{\varphi}_1 \\ \ddot{\varphi}_2 \end{bmatrix} = [Q] \tag{36}$$

Model verification and simulation tests

The dynamic model of the shearer with a chain haulage system, expressed by means of equations, enables determining the number of quantities that describe its behaviour and load (Kopas et al., 2017). Due to the complexity of the obtained equations, it is saved in the form of scripts in the Matlab environment. The differential equations were solved by the fourth-order Runge-Kutta method.

An important step was the verification of the developed model. Preliminary tests were carried out using the created model to verify the correctness of the scripts and formulas.

The model described can be divided into several elements that have been tested independently:

- cutting resistance,
- resistance to motion,
- free movement of the solid,
- initial tension of the chain,
- change in the length of individual chain branches.

An example of a diagram showing a chain tension analysis is shown in Fig. 13. The oscillations of the drive wheel and the shearer's centre of gravity indicate that the chain is not properly tensioned, which causes undesirable motion.

$$[Q]=\begin{bmatrix} P_x \\ P_y \\ \frac{1}{3}\rho\dot{\varphi}_2\dot{z}_s r+\frac{1}{3}\rho\dot{\varphi}_2\dot{\varphi}_x y_p r+\frac{1}{3}\rho\dot{\varphi}_2\dot{\varphi}_y x_p r+\frac{1}{6}\rho\dot{\varphi}_2^2 r^2-\frac{1}{3}\rho\dot{\varphi}_1\dot{z}_s r-\frac{1}{3}\rho\dot{\varphi}_1\dot{\varphi}_x y_p r-\frac{1}{3}\rho\dot{\varphi}_1\dot{\varphi}_y x_p r-\frac{1}{6}\rho\dot{\varphi}_1^2 r^2+P_z \\ \frac{1}{3}\rho\dot{\varphi}_2\dot{z}_s y_p r+\frac{1}{3}\rho\dot{\varphi}_2\dot{\varphi}_x y_p^2 r+\frac{1}{3}\rho\dot{\varphi}_2\dot{\varphi}_y x_p y_p r+\frac{1}{6}\rho\dot{\varphi}_2^2 y_p r^2-\frac{1}{3}\rho\dot{\varphi}_1\dot{z}_s y_p r-\frac{1}{3}\rho\dot{\varphi}_1\dot{\varphi}_x y_p^2 r-\frac{1}{3}\rho\dot{\varphi}_1\dot{\varphi}_y x_p y_p r-\frac{1}{6}\rho\dot{\varphi}_1^2 y_p r^2+M_x \\ \frac{1}{3}\rho\dot{\varphi}_2\dot{z}_s x_p r+\frac{1}{3}\rho\dot{\varphi}_2\dot{\varphi}_x y_p x_p r+\frac{1}{3}\rho\dot{\varphi}_2\dot{\varphi}_y x_p^2 r+\frac{1}{6}\rho\dot{\varphi}_2^2 x_p r^2-\frac{1}{3}\rho\dot{\varphi}_1\dot{z}_s x_p r-\frac{1}{3}\rho\dot{\varphi}_1\dot{\varphi}_x y_p x_p r-\frac{1}{3}\rho\dot{\varphi}_1\dot{\varphi}_y x_p^2 r-\frac{1}{6}\rho\dot{\varphi}_1^2 x_p r^2+M_y \\ M_z \\ \frac{1}{6}\rho r\left[\left(\dot{z}_s+\dot{\varphi}_x\cdot y_p+\dot{\varphi}_y\cdot x_p\right)^2+\dot{\varphi}_1^2 r^2+\dot{\varphi}_1 r\left(\dot{z}_s+\dot{\varphi}_x\cdot y_p+\dot{\varphi}_y\cdot x_p\right)\right]-\frac{1}{3}\rho\dot{\varphi}_1^2 r^3-\frac{1}{6}\rho\dot{\varphi}_1\dot{z}_s r^2-\frac{1}{6}\rho\dot{\varphi}_1\dot{\varphi}_x y_p r^2\ldots \\ -\frac{1}{6}\rho\dot{\varphi}_1\dot{\varphi}_y x_p r^2-\frac{1}{6}\rho\left(\dot{\varphi}_2 r-\dot{\varphi}_1 r\right)\left(2\dot{\varphi}_1 r^2+\dot{\varphi}_2 r^2\right)-\frac{1}{6}\rho r\left(\dot{\varphi}_1^2 r^2+\dot{\varphi}_2^2 r^2+\dot{\varphi}_1\dot{\varphi}_2 r^2\right)+M_1 \\ \frac{1}{6}\rho\dot{\varphi}_2 r\left(2\dot{\varphi}_2 r^2+\dot{z}_s r+\dot{\varphi}_x y_p r+\dot{\varphi}_y x_p r\right)-\frac{1}{6}\rho r\left[\left(\dot{z}_s+\dot{\varphi}_x y_p+\dot{\varphi}_y x_p\right)^2+\dot{\varphi}_2^2 r^2+\dot{\varphi}_2 r\left(\dot{z}_s+\dot{\varphi}_x y_p+\dot{\varphi}_y x_p\right)\right]\ldots \\ -\frac{1}{6}\rho\left(\dot{\varphi}_2 r-\dot{\varphi}_1 r\right)\left(2\dot{\varphi}_2 r^2+\dot{\varphi}_1 r^2\right)+\frac{1}{6}\rho r\left(\dot{\varphi}_1^2 r^2+\dot{\varphi}_2^2 r^2+\dot{\varphi}_1\dot{\varphi}_2 r^2\right)+M_2 \end{bmatrix} \tag{37}$$

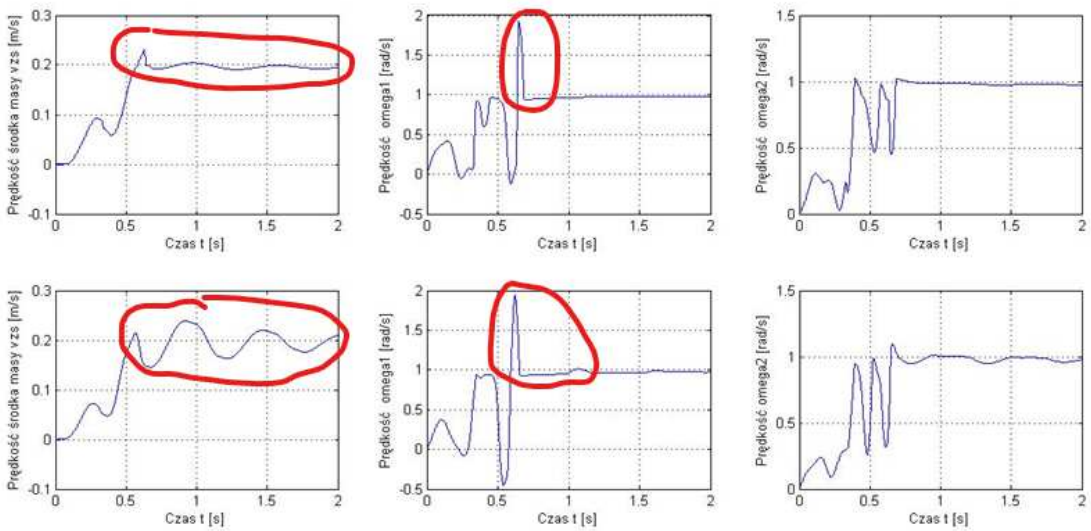

Fig. 13. Changes in values of the speed of the shearer's advance and the sprockets over time for an improperly tensioned chain

After checking its correct operation, the developed model of a single-cutting head shearer was used to perform the required shearer loading tests (Wiecek et al., 2019).

The analysis of the single-cutting head longwall shearer's load required specifying the values of important parameters. Parameters of the following model elements were determined or assumed:

- longwall working (length, height, slope) and longwall shearer (mass, moments of inertia, dimensions),
- chain with a sprocket (stiffness, linear density, moment of inertia, equivalent radius),

- motor (power, locked and breakdown torque, rated and critical speed, moment of inertia),
- friction coefficients and parameters of the coal face (density, workability),
- pick system of the cutting head (arrangement and number of picks, cutting angles).

Next, the developed model of a single-cutting head shearer, which had been checked for correct operation, was used to perform the required shearer loading tests (Burduk et al., 2019). The values of the significant parameters of the tested object were determined and accepted; qualitative and quantitative tests were carried out. The research results were presented in the author's article (Bołoz, 2018).

Summary

A significant share of thin hard coal seams and the high costs of their extraction provide arguments for seeking new opportunities for their profitable exploitation while maintaining the required safety and comfort of the staff. Due to their design and method of operation, longwall shearers and coal ploughs for exploiting thin hard coal seams that are currently available on the market do not allow achieving the assumed daily extraction under difficult mining and geological conditions. The proposed complex solves a number of problems related to the exploitation of the discussed seams. The presented solution is a new design, significantly differing from the currently produced longwall shearers, which necessitates many changes in the design of cooperating machines in order to create a number of compatible devices used in a specialised shearer system for the exploitation of thin seams.

Due to the lack of appropriate models, it was necessary to develop a proprietary mathematical model that would allow assessing the behaviour and load of the single-cutting headcutting shearer. The developed model differs from the known models designed to analyse longwall shearers and ploughs with a chain haulage system. It takes into account the six degrees of freedom of the shearer as well as the continuously and evenly distributed mass of the chain. In addition, the weights of individual segments of the chain change during the shearer's operation. Description of the chain segments as elements with a continuously distributed mass allows simulating the start-up of the shearer and analysis during its entire advance from the beginning to the end of the longwall. No other model makes it possible to simulate the shearer's advance – other solutions merely enable a point analysis at specific locations of the longwall.

The discussed formulas have been based on the author's original mathematical model that allows for determining the cutting resistance while taking into account also the turned picks located on the cut-off disc.

However, attention should be paid to the limitations of the discussed dynamic model. Due to the fact that the sprocket has been simplified and chain segments have been described with a continuous model, the considered model is not suitable for a detailed analysis of the drive or the chain itself. Neither can it be used to analyse the transverse vibrations of the chain. However, both phenomena have little impact on the dynamics of the shearer. Therefore, the above-mentioned simplifications are not significant limitations.

The single-cutting head shearer with a chain haulage system has some features in common with static coal ploughs as well as scraper or belt conveyors. The developed model can be successfully used for developing a dynamic model of these machines, especially in terms of describing the dynamics of the chain used in scraper conveyors and ploughs as well as the belt used in belt conveyors.

References

Abd Ali, L.M., Ali, Q.A., Klačková, I., Issa, H.A., Yakimovich, B.A., Kuvshimov, V. (2021). Developing a thermal design for steam power plants by using concentrating solar power technologies for a clean environment. Acta Montanistica Slovaca, vol. 26 (4), 2021, pp. 773-783, 2021, DOI https://doi.org/10.46544/AMS.v26i4.14, 2021

Abramov, I., Bozek, P., Nikitin, Y., Abramov, A., Sosnovich, E., Stollmann. (2015). Diagnostics of electrical drives. In The 18th International Conference on Electrical Drives and Power Electronics . EDPE 2015. The High Tatras, Slovakia, 21 - 23. September 2015, pp. 364-367. DOI: 10.1109/EDPE.2015.7325321

Bedoustani, Y., Birgas, P., Taghirad, H. and Bonev I. (2011). Lagrangian Dynamics of cable-driven parallel manipulators: a variable mass formulation. Transactions of the Canadian Society for Mechanical Engineering, 35(4), pp. 1-11.

Biały, W. (2014). Coal cutting force measurement system – (CCFM). *14th SGEM GeoConference on Science and Technologies In Geology, Exploration and Mining, SGEM2014 Conference Proceedings*, ISBN 978-619-7105-09-4/ISSN 1314-2704 June 17-26, Vol. III, pp. 91-98,

Biały, W. (2016). Determination of workloads in cutting head of longwall tumble heading machine. *Management Systems in Production Engineering*, 1, pp. 45-54.

Bołoz, Ł. (2013). Unique project of single-cutting head longwall shearer used for thin coal seams exploitation, *Archives of Mining Sciences.* 58(4), pp. 1057-1070.

Bołoz, Ł. (2018). Model tests of longwall shearer with string feed system, *Archives of Mining Sciences.* 63(1), pp. 61-74.

Bołoz, Ł. (2020). Static and dynamic calculations of suspended monorails' selected parameters. *Acta Montanistica Slovaca*, 26(3), pp. 566-581.

Bołoz, Ł. and Biały, W. (2020). Automation and Robotization of Underground Mining in Poland, *Applied Sciences.*10(20), pp. 1-14.

Bołoz, Ł. and Castañeda, L. (2018). Computer-aided support for the rapid creation of parametric models of milling units for longwall shearers. *Management Systems in Production Engineering*. 26(4), pp. 193–199.

Bołoz, Ł. and Kozłowski, A. (2021) Methodology for Assessing the Stability of Drilling Rigs Based on Analytical Tests, *Energies*, 14(24), pp. 1-29.

Bortnowski, P., Gładysiewicz, L., Król, R. and Ozdoba, M. (2021). Models of Transverse Vibration in Conveyor Belt—Investigation and Analysis. *Energies*. 14(14), pp. 1-14.

Bozek, P., Nikitin, Y., Krenicky, T. (2022). Diagnostics of Mechatronic Systems. Springer International Publishing, 2021 ; Cham. 150 pp. Studies in Systems, Decision and Control; Vol. 345. <https://www.springer.com/gp/book/9783030670542>. DOI: 10.1007/978-3-030-67055-9

Burduk, A., Wiecek, D., Tlach, V., Ságová, Z., Kochanska, J. (2021). Risk assessment of horizontal transport system in a copper mine. Acta Montanistica Slovaca, vol. 26 (2), 2021, DOI 10.46544/AMS.v26i2.09, 2021

Cheluszka, P. (2021). Numerical Studies of the Dynamics of the Roadheader Equipped with an Automatic Control System during Cutting of Rocks with Different Mechanical Properties. *Energies.*14(21), pp. 1-29.

Cheluszka, P., Kaula, R., Heyduk, A. and Gawlik, J. (2018). Modelling the dynamics of a drive of boom-Type roadheader cutting heads at adjustable angular speed. *Archives of Mining Sciences.* 63(1), pp. 183-204.

Derlukiewicz, D., Karliński, J. (2012). Static and dynamic analysis of telescopic boom of self-propelled tunnelling machine. *Journal of Theoretical and Applied Mechanic.* 50(1), pp. 47-59.

Dolipski, M., Remiorz, E. and Sobota, P. (2012). Determination of dynamic loads of sprocket drum teeth and seats by means of a mathematical model of the longwall conveyor. *Archives of Mining Sciences.* 57(4), pp. 1104-1119.

Dolipski, M., Remiorz, E. and Sobota, P. (2014). Dynamics of Non-Uniformity Loads of Afc Drives. *Archives of Mining Sciences,* 59(1), pp. 156-168.

Handrik, M., Kopas, P., Baniari, V., Vasko, M., Saga, M. (2017). Analysis of stress and strain of fatigue specimens localised in the cross-sectional area of the gauge section testing on bi-axial fatigue machine loaded in the high-cycle fatigue region. XXI Polish-Slovak Scientific Conference Machine Modeling and Simulations MMS 2016, Hucisko, Poland, 6-8 sept. 2016, Procedia Engineering, vol. 177, pp. 516-519, DOI 10.1016/j.proeng.2017.02.254, 2017

Hou, Y., Fang, P., Nan, Y. and Du, M. (2016). Synchronization investigation of vibration system of two co-rotating rotor with energy balance method. *Advances in Mechanical Engineering*. 8(1), pp. 1-19.

Jakubowski, J. and Peterka, J. (2014). Design for manufacturability in virtual environment using knowledge engineering. *Management and production engineering review*. 5(1), pp. 3-10,

Jedliński, Ł., Syta, A., Gajewski, J. and Jonak, J. (2022). Nonlinear analysis of cylindrical gear dynamics under varying tooth breakage, *Measurement,* 190, pp. 1-13.

Jiang, S., Zhang, X., Gao, K., Gao, J., Wang, O. and Hidenori. K. (2017). Multi-Body Dynamics and Vibration Analysis of Chain Assembly in Armoured Face Conveyor. *International Journal of Simulation Modelling*. 16, pp. 458-470.

Jonak, J., Kuric, I., Droździel, D., Gajewski, J. and Saga, M. (2020). Prediction of load on the cutting tools in tunnel boring machines. *Acta Montanistica Slovaca*, (4), pp. 444-452.

Junxia, L. and Xiaoxu P. (2018). Belt Conveyor Dynamic Characteristics and Influential Factors. *Shock and Vibration*. 11, pp. 1-13.

Kang, X. and Li, G. (2010). Multi-DOF dynamic model for a coal plough with its simulation. *Journal of China Coal Society* 29. 139-144.

Karliński, J., Ptak, M., Chybowski, L. (2020) Simulation-Based Methodology for Determining the Dynamic Strength of Tire Inflation Restraining Devices. *Energies*. 13(4), pp. 1-14.

Karliński, J., Stańco, M., Działak, P. (2017). Determination of the dynamic overloads in the loader structure. Materials Today-Proceedings, pp. 5843-5848.

Klarák, J., Andok, R., Hricko, J., Klačková, I., Tsai, H.-Y. (2022). Design of the Automated Calibration Process for an Experimental Laser Inspection Stand. Sensors 2022, 22, 5306, https://doi.org/10.3390/s22145306, 2022

Kopas, P., Blatnicky M., Saga M., Vasko, M. (2017). Identification of mechanical properties of weld joints of AlMgSi07.F25 Aluminium Alloy. Metalurgija, vol. 56 (1-2), 2017, pp. 99-102, 2017

Kopas, P., Saga, M., Baniari, V., Vasko, M., Handrik, M. (2017). A plastic strain and stress analysis of bending and torsion fatigue specimens in the low-cycle fatigue region using the finite element methods. XXI Polish-Slovak Scientific Conference Machine Modeling and Simulations MMS 2016, Hucisko, Poland, 6-8 sept. 2016, Procedia Engineering, vol. 177, pp. 526-531, DOI 10.1016/j.proeng.2017.02.256, 2017

Kotwica, K., Stopka, G., Kalita, M., Bałaga, D. and Siegmund, M. (2021). Impact of Geometry of Toothed Segments of the Innovative KOMTRACK Longwall Shearer Haulage System on Load and Slip during the Travel of a Track Wheel. *Energies*. 14(9), pp. 1-25.

Kouroussis, G., Connolly, D., Vogiatzis, K. and Verlinden, O. (2015). Modelling the Environmental Effects of Railway Vibrations from Different Types of Rolling Stock: A Numerical Study. *Shock and Vibration*. Article ID 142807.

Kovanič, L.; Blišťan, P., Zelizňaková, V., Palková, J., Baulovič, J.: Deformation investigation of the shell of rotary kiln using terrestrial laser scanning (TLS) measurement, Metalurgija 58 (3-4), 2019, pp 311-314, ISSN 1334-2576

Kovanič, Ľ.; Ambriško, Ľ.; Marasová, D.; Blišťan, P.; Kasanický, T.; Cehlár, M. Long-Exposure RGB Photography with a Fixed Stand for the Measurement of a Trajectory of a Dynamic Impact Device in Real Scale. *Sensors* 2021, *21*, 6818. https://doi.org/10.3390/s21206818

Kovanič, Ľ., Blistan, P., Rozložník, M. and Szabó, G. UAS RTK / PPK photogrammetry as a tool for mapping the urbanized landscape, creating thematic maps, situation plans and DEM. Acta Montanistica Slovaca. 2021, Volume 26 (4) 649-660 DOI: https://doi.org/10.46544/AMS.v26i4.05

Kovanič, Ľ.; Blistan, P.; Urban, R.; Štroner, M.; Pukanská, K.; Bartoš, K.; Palková, J. Analytical Determination of Geometric Parameters of the Rotary Kiln by Novel Approach of TLS Point Cloud Segmentation. Appl. Sci. 2020, 10, 7652

Kuric, I., Klačková, I., Domnina, K., Stenchlák, V., Sága, M. jr. (2022). Implementation of Predictive Models in Industrial Machines with Proposed Automatic Adaptation Algorithm. Applied Sciences - Basel, Mdpi, 2022, vol. 12 (4), 1853, ISSN 2076-3417, DOI.org/10.3390/app12041853, 2022

Kuric, I., Klačková, I., Nikitin, Y.R., Zajačko, I., Císar, M., Tucki, K. (2021). Analysis of diagnostic methods and energy of production systems drives, Processes, Mdpi, 9, 843, DOI.org/10.3390/pr9050843, 2021

Kuric, I., Tlach, V., Císar, M., Ságová, Z., Zajačko, I. (2020). Examination of industrial robot performance parameters utilizing machine tool diagnostic methods. In International Journal of Advanced Robotic Systems, 17 (1), 2020, DOI 10.1177/1729881420905723, 2020

Li, X. Liu, X., Jiao, L., Do, T. (2010). Dynamic simulation of sliding coal plough under different working conditions. *Journal of China Coal Society*. 35, 1202-1206.

Litak G., Syta A., Gajewski J. and Jonak J. (2010). Detecting and identifying non-stationary courses in the ripping head power consumption by recurrence plots, *Meccanica*, 45, pp. 603–608.

Liu, C., Qin, D., and Liao, Y. (2015). Electromechanical dynamic analysis for the drum driving system of the long-wall shearer. *Advances in Mechanical Engineering*. 7(1), pp. 1-14.

Lohrengel, A., Kramarczyk, W., Kruk, R. and Wieczorek, A. (2011). Modelling dynamic phenomena in gear transmissions using the rigid element method. *Górnictwo i geologia*. 6(3), pp. 115-126.

Midor, K. (2017). Innovation in coal mining management as an intelligent specialization, Production Engineering Archives, 15, pp. 41-44.

Muravev, V. V., Muraveva, O. V., Volkova, L. V., Sága, M., Ságová, Z. (2019). Measurement of Residual Stresses of Locomotive Wheel Treads During the Manufacturing Technological Cycle. Management systems in Production Engineering, 27 (4) 2019, DOI 10.1515/mspe-2019-0037, 2019

Nikitin, Y., Bozek, P. and Peterka, J. (2020). Logical-Linguistic Model of Diagnostics of Electric Drives with Sensors Support. *Sensors*. 20(16), Article Number: 4429

Pesce, C. (2003). The application of Lagrange equations to mechanical systems with mass explicitly dependent on position. *Journal of Applied Mechanics*, 70(5), pp. 751-756.

Pesce, C., Tannuri, E. and Casetta L. (2006). The Lagrange equation for systems with mass varying explicitly with position: some applications to offshore engineering. *Journal of the Brazilian Society of Mechanical Sciences and Engineering*, 28(4), pp. 496-504.

Peterka, J. Nikitin, Y. and Bozek, P. (2020). Diagnostics of automated technological devices. *MM Science Journal*. Pp. 4027-4034.

Prostański, D. (2012). Dust control with use of air-water spraying system. *Archives of Mining Sciences*, 4, pp. 975-990.

Saga M., Blatnicka M., Blatnicky M., Dizo J., Gerlici J. (2020). Research of the Fatigue Life of Welded Joints of High Strength Steel S960 QL Created Using Laser and Electron Beams, Materials, vol.13 (11), Article No. 2539, DOI 10.3390/ma13112539, 2020

Saga M., Blatnicky M., Vasko M., Dizo J., Kopas P., Gerlici J. (2020). Experimental Determination of the Manson-Coffin Curves for an Original Unconventional Vehicle Frame. Materials, vol.13 (20), Article No. 4675, DOI 10.3390/ma13204675, 2020

Saga M., Jakubovicova L. (2014). Simulation of vertical vehicle non-stationary random vibrations considering various speeds, Scientific Journal of Silesian University of Technology-Series Transport. Vol. 84, pp. 113-118, 2014

Saga, M., Vasko, M. (2009). Stress sensitivity analysis of the beam and shell finite elements. Komunikacie, vol. 11 (2), pp 5-12, ISSN 1335-4205, 2009

Saga M., Vasko, M., Pechac, P.(2014). Chosen numerical algorithms for interval finite element analysis. Modelling of Mechanical and Mechatronic Systems, MMaMS 2014, Vysoké Tatry, Slovakia, 25-27 nov. 2014, Procedia Engineering, vol. 96, pp. 400-409, DOI 10.1016/j.proeng.2014.12.109, 2014

Sapietova, A., Saga, M., Novak, P., Bednar, R., Dizo, J. (2011). Design and Application of Multi-software Platform for Solving of Mechanical Multi-body System Problems. Mechatronics: Recent Technological and Scientific Advances. 9th International Conference on Mechatronics, Warsaw, Poland, sep. 21-24, 2011, pp. 345-354, 2011

Segota, SB., Andelic, N., Lorencin, I., Saga M., Car, Z. (2020). Path planning optimization of six-degree-of-freedom robotic manipulators using evolutionary algorithms. International journal of advanc*ed robotic systems, vol.17 (2)*, DOI 10.1177/1729881420908076, 2020

Sentyakov, K., Peterka, J., Smirnov, V., Bozek, P., Sviatskij, V. (2020). Modeling of Boring Mandrel Working Process with Vibration Damper. In Materials Vol. 13, iss. 8 (2020), pp.1-13. DOI: 10.3390/ma13081931

Tlach, V., Kuric, I., Ságová, Z., Zajačko, I. (2019). Collaborative assembly task realization using selected type of human-robot interaction. In; 13th International Scientific Conference on sustainable, modern and safe transport (Transcom 2019), Book Series Transportation Research Procedia, 40 (2019), DOI 10.1016/j.trpro.2019.07.078, 2019

Wiecek, D., Burduk, A., Kuric, I. (2019). The use of ANN in improving efficiency and ensuring the stability of the copper ore mining process. Acta Montanistica Slovaca, vol. 24 (1), pp. 1–14, 2019.

Yang, H., Li, W., Luo, C., Zhang, J. and Si, Z. (2016). Research on Error Compensation Property of Strapdown Inertial Navigation System Using Dynamic Model of Shearer. IEEE Access. 4:1-1. pp. 2045-2055.

Yang, X., Zou, X., Zhang, S., Chen, H., Wei, Y. and Li, P. (2021). Dynamical behavior of coal shearer under the influence of multiple factors in slant-cutting conditions. *Scientific reports.* 11(1), pp. 1-18.

Zajačko, I., Gál, T., Ságová, Z., Mateichyk, V., Wiecek, D. (2018) Application of artificial intelligence principles in mechanical engineering. In; Innovative technologies in Engineering production (ITEP´18), Book Series: MATEC Web of Conferences, Vol. 244, article no. 01027, 3rd International Scientific Conference on Innovative Technologies in Engineering Production (ITEP), 11-13 September 2018, Bojnice, Slovakia DOI 10.1051/matecconf/201824401027, 2018

Zasadzień, M. and Midor, K. (2015). Innovative application of quality management tools in a hard coal mine. *15th International Multidisciplinary Scientific GeoConference SGEM 2015. Science and technologies in geology, exploration and mining. Vol. 3, Exploration and mining, applied and environmental geophysics.* Sofia: STEF92 Technology, pp. 415-421.

Zhang, R., Zhang, Y. (2020). Dynamic model and analysis of the traction unit gear system in long wall coal shearer. *Proceedings of the Institution of Mechanical Engineers, Part K: Journal of Multi-body Dynamics.* 234(3), pp. 546-567.